

Article

Nutrient Flux under the Influence of Melt Water Runoff from Volcanic Territories and Ecosystem Response of Vilyuchinskaya and Avachinskaya Bays in Southeastern Kamchatka

Pavel Semkin ^{*}, Galina Pavlova, Vyacheslav Lobanov, Yuri Barabanshchikov, Sergey Kukla, Sergey Sagalaev, Maria Shvetsova, Elena Shkirknikova, Petr Tishchenko, Evgenia Tibenko, Olga Ulanova and Pavel Tishchenko

Il'ichev Pacific Oceanological Institute, Far Eastern Branch, Russian Academy of Sciences, Vladivostok 690041, Russia; pavlova@poi.dvo.ru (G.P.); lobanov@poi.dvo.ru (V.L.); biw90@mail.ru (Y.B.); kukla.sp@poi.dvo.ru (S.K.); sagalaev@poi.dvo.ru (S.S.); chippers@rambler.ru (M.S.); elmi@poi.dvo.ru (E.S.); eq15@poi.dvo.ru (P.T.); tibenko@poi.dvo.ru (E.T.); ulanova@poi.dvo.ru (O.U.); tpavel@poi.dvo.ru (P.T.)

* Correspondence: pahno@list.ru; Tel.: +7-9146647833

Abstract: Nutrient fluxes with river runoff can largely determine the state of coastal water ecosystems. The Vilyuchinskaya and Avachinskaya Bays of Kamchatka Peninsula were surveyed on 4–5 July 2022, just after the peak of the spring–summer flood of the Vilyucha and Avacha Rivers associated with the snow melting in volcanic areas. Additionally, water sampling was performed in river water in December 2022, in the period of winter low water. A general undersaturation of CO₂ of surface waters was observed in the Vilyuchinskaya and Avachinskaya Bays. Strong supersaturation of CO₂ of the near-bottom waters was observed, due to microbial destruction of organic matter, especially in Avachinskaya Bay. This organic matter was formed as a result of photosynthesis in the water column, which subsequently gravitated to the bottom and concentrated in specific bottom depressions in the studied bays. In these depressions, black sediments were found, in which sulfate reduction occurred. The porewater of sediments had a very high concentration of organic carbon, dissolved and organic nitrogen, and phosphates, as well as CO₂ partial pressure. The source of nutrients for the studied bays is tephra (volcanic suspended particles), which covers all the watersheds, including the soil and snow, as a result of volcanic activity in the study region. Based on the calculated nutrient fluxes in river runoff for the summer and winter seasons and the DIN/DIP ratios in river, sea, and pore waters, the causes of phytoplankton blooms, including the occurrence of red tides, are discussed. The maximum flux of nutrients and, accordingly, phytoplankton blooms should be expected in the years with the highest volcanic activity and high summer air temperatures, since the melting of nutrient-rich snow and ice will be maximum. This will determine the flux of nutrients in the river runoff of the Kamchatka Peninsula and contribute to phytoplankton blooms.

Keywords: Kamchatka Peninsula; estuary; CO₂; nutrient flux; phytoplankton bloom; organic matter; snow cover; volcanic ash



Citation: Semkin, P.; Pavlova, G.; Lobanov, V.; Barabanshchikov, Y.; Kukla, S.; Sagalaev, S.; Shvetsova, M.; Shkirknikova, E.; Tishchenko, P.; Tibenko, E.; et al. Nutrient Flux under the Influence of Melt Water Runoff from Volcanic Territories and Ecosystem Response of Vilyuchinskaya and Avachinskaya Bays in Southeastern Kamchatka. *J. Mar. Sci. Eng.* **2023**, *11*, 1299. <https://doi.org/10.3390/jmse11071299>

Academic Editor: Weidong Zhai

Received: 25 May 2023

Revised: 22 June 2023

Accepted: 23 June 2023

Published: 26 June 2023



Copyright: © 2023 by the authors. Licensee MDPI, Basel, Switzerland. This article is an open access article distributed under the terms and conditions of the Creative Commons Attribution (CC BY) license (<https://creativecommons.org/licenses/by/4.0/>).

1. Introduction

Nutrient flux in the river runoff in coastal basins is inseparably linked with such currently topical problems as eutrophication [1–3], phytoplankton bloom outbreaks, and red tide events [4–7], as well as hypoxia and anoxia [8–10]. Variation of the DIN/DIP ratio and increases in organic matter (OM) concentrations may be the main reason for dinoflagellate blooms, including their toxic species [11–16].

OM production/destruction affects nitrogen and phosphorus ($\text{NO}_2^- + \text{NO}_3^- + \text{NH}_4^+ = \text{DIN}$, PO_4^{3-} (DIP)), as well as silicon (DSi), as the main CO₂ consumers in the world's oceans are diatomic algae [17], normally dominating over dinoflagellates [18]. The carbonate system

is a chemical reaction that occurs as a consequence of the interaction of CO₂ with a water molecule. Accordingly, the parameters of the carbonate system determine the state of the balance of production/destruction of OM and thus determine the state of the ecosystem. The partial pressure of carbon dioxide (pCO₂) is one of the most important indicators in the production/destruction balance cycle of carbon (C) studies, along with the other parameters of the carbonate system (pH, total alkalinity (TA), and dissolved inorganic carbon (DIC) ($\text{DIC} = [\text{CO}_2] + [\text{HCO}_3^-] + [\text{CO}_3^{2-}]$) [19].

Volcanic ash (tephra) becomes enriched with nutrients and iron (Fe) due to volcanic gas condensation and the adsorption of aerosols on particles during eruptions [20,21]. Experiments on bioincubation showed that microalgae are capable of using nutrients that appear when tephra is added to water [22]. The experimental enrichment with Fe of oceanic waters was also accompanied by increased primary production [23,24]. In locations where tephra had fallen into the ocean, a phytoplankton bloom was observed [25–29], and the balance of CO₂ in the water column and bottom sediments changed [30–33]. This means that tephra can contribute to strengthening the biological pump for atmospheric CO₂ and contribute to its overall reduction on the planet [34]. However, experiments on the release of the salts of metals and nutrients demonstrated different concentrations of these substances with different tephra characteristics when entering the sea and fresh water [35]. Perhaps, this will result in differences in the flux of substances in river discharges, due to the diversity of drainage basins in volcanic territories.

It is known that phytoplankton blooms regularly occur off East Kamchatka due to continental discharges [36,37], and red tides are observed [38,39]. These red tides can block the migration of salmon to the rivers of the East Kamchatka, which has been considered a major economic problem in some years [39], because it is one of the world's most important fishing regions. The sources and routes of nutrients to the coastal basins of this area have not been fully identified.

The purpose of this paper is to study the behavior of nutrients, as well as their complex of characteristics, showing the intensity and direction of the OM production/destruction balance, including parameters of the carbonate system in the water and bottom sediments of the Vilyuchinskaya and Avachinskaya Bays that are influenced by Vilyucha R. and Avacha R.

2. Materials and Methods

2.1. Study Area

The most active volcanoes in East Kamchatka region are Shiveluch, Klyuchevskoy, Bezemyannyi, Ploskiy Tolbachik, Karymskiy, Avachinskiy, Koryakskiy, Gorelyi, and Mutnovskiy. There are volcanoes of the Avacha group located in our study area (Figure 1), two of which—Avachinskiy and Koryakskiy—are active and form part of the left-bank drainage basin of Avacha R. The height of the Avachinskiy and Koryakskiy volcanoes is 2741 and 3456 m, respectively. The 2173-meter-high Vilyuchinskiy volcano, forming part of the left-bank drainage basin of Vilyucha R., is extinct. Nevertheless, the release of gases and fumes was repeatedly observed on its summit, and there is a network of hydrothermal springs in its lower part in the Vilyucha R. valley. The estuaries under consideration are located in the ash fall zone, where tephra spreads over a distance of hundreds of kilometers from the active volcanoes. The amount of tephra produced by one eruption of the Avachinskiy volcano can reach several thousands of tons per 1 km² [40]. That is why the volcanic soil type dominates in the drainage basins of the rivers under consideration [41]. Due to below-zero mean yearly temperatures and a large amount of precipitation (Table 1), the region under consideration is covered with snow 180–300 days of the year and there are permafrost and glaciers covered with tephra in highland areas [41].

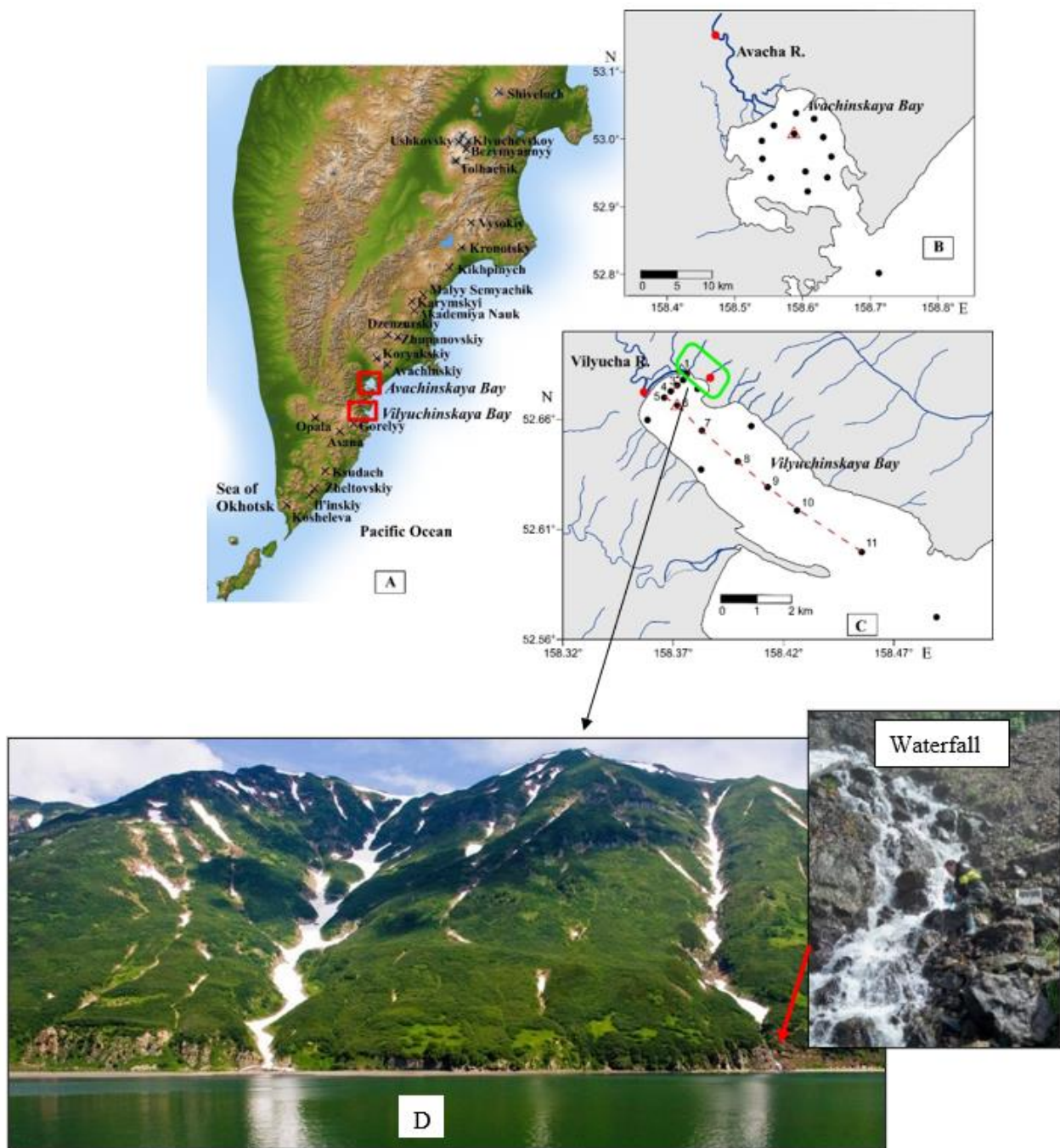


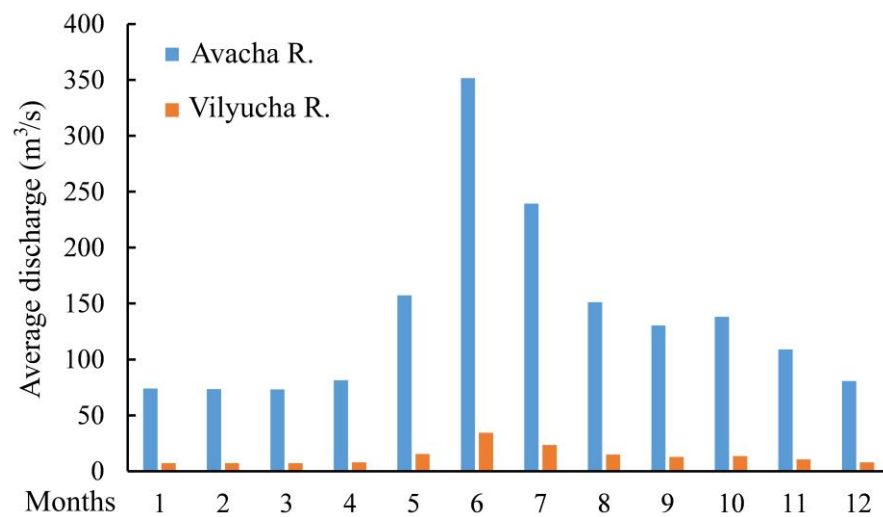
Figure 1. The study area and active volcanoes (X)—(A), locations of stations in Avachinskaya and Vilyuchinskaya Bays—(B) and (C) respectively, (D)—mountain slope on the left bank of the Vilyucha R. valley and Vilyuchinskaya Bay. ●—river water sampling stations, Δ—stations where bottom sediment samples were taken. The red dotted line in “(C)” is an oceanographic profile, St. 1–11.

The Avacha River is a relatively large river on the southeastern coast of Kamchatka. Its length is 122 km, its drainage basin square area is 5090 km², and its mean yearly flow rate during 2008–2020 was 138 m³/c (<https://gmvo.skniivh.ru/>) accessed on 1 January 2023). The rivers of the study area, including Avacha R., are primarily snow-fed and the key phase of their water regime is the spring–summer high water conditions during May–July, which account for 70% of their yearly runoff. The water flow rate normally increases from early May and has two level peaks. The first peak is small and is caused by snow and ice melting in river valleys; and the second peak, the main one, is caused by snow and ice melting in

highland areas and occurs in late June–early July (Figure 2). Maximum yearly flow rates are observed during the second peak, up to 940 m³/s (as per 2013 data), with the mean flow rates during 2008–2020 being 351.4 and 239.4 m³/s for June and July, respectively. The lowest flow rates are observed in December–February, when the mean monthly values vary in the range of 80 to 74 m³/s.

Table 1. Average data over a period of many years: precipitation rate, mm; air temperature, °C and snow cover height (cm) at Petropavlovsk Point—lighthouse (120 m above sea level) [42].

	Months												In a Year
	1	2	3	4	5	6	7	8	9	10	11	12	
Amount of Precipitation	108	84	167	110	66	64	93	96	93	115	174	111	1280
Temperature	−6.1	−5.4	−3.2	0.7	5.6	10.7	14.3	15.3	11.1	6.0	−0.5	−4.7	3.6
Snow thickness	70	83	84	83	18	0	0	0	0	0	11	44	



Max. Discharge	Avacha R.	96.8	99.9	93.9	160	472	940	653	317	368	367	202	222
	Vilyucha R.	9.5	9.8	9.2	15.7	46.4	92.3	64.1	31.1	36.1	36.1	19.8	21.8
Min. Discharge	Avacha R.	53.1	53.1	55.7	61.4	72.4	151	111	93	90.4	86	47.7	47.7
	Vilyucha R.	5.2	5.2	5.5	6.0	7.1	14.8	10.9	9.1	8.9	8.4	4.7	4.7

Figure 2. Mean, maximum, and minimum water flow rates in the Avacha River and Vilyucha River over a multi-year period (2008–2020) (estimates are based on Avacha’s mean daily flow rates (<https://gmvo.skniivh.ru/>) accessed on 1 January 2023).

The Vilyucha River is a mountainous river 26 km long. Its drainage basin square area is about 500 km². As there are no stream gauging stations on this river, a factor of the square area relation of Avacha R./Vilyucha R. = 10.18 was use. According to this rough estimate, Vilyucha’s mean yearly runoff is 13.6 m³/s, its runoff in June and July is 35.5 and 23.5 m³/s, respectively, and that during December–February is about 7 m³/s. In this paper, we used approximate water flow rates in Avacha and Vilyucha Rivers of 288 and 28 m³/s for our summer expedition and 77 and 7 m³/s for December 2022.

Ice phenomena in the rivers of the study area are observed during early November–early May, i.e., the ice coverage period is 150–170 days of the year.

In the drainage basin of Avacha R., an additional flux of nutrients may originate from the city of Yelizovo, with a population of 36,000 persons. The drainage basin of Vilyucha R. is of a mountainous and taiga type, with no populated places in this area. This allows the study of natural processes in Vilyuchinskaya Bay, unaffected by human-induced impacts.

2.2. Field Work, Hydrological Surveys, and Water Sampling

The results of the expedition by the Pacific Oceanological Institute, Far Eastern Branch of the Russian Academy of Sciences, in 2022 after the peak of spring–summer high water conditions are presented. Sampling was performed in the estuary of Vilyucha R. on 4 July and in the estuary of Avacha R. on 5 July. Water samples were taken from on board the research vessel *Professor Gagarinsky* in Avachinskaya and Vilyuchinskaya Bays and from a speed boat in the Avacha and Vilyucha Rivers. Water samples were also taken in one of seasonal waterfalls on the shore of Vilyuchinskaya Bay, emerging due to snow melting on the mountain range slopes (Figure 1).

The second water sampling operation was performed in the course of the winter expedition on board the research vessel *Academic Oparin* from December 12th to 16th. As for this expedition's findings, in our paper, we only analyze the river water characteristics, without considering the mixing zone as a whole.

This paper presents the following measured characteristics: salinity, temperature, pH, TA, nutrients in mineral form DIP, DSi, DIN, sum of minerals, and organic forms of nitrogen (N_{tot}) and phosphorus (P_{tot}) ($N_{\text{tot}} = \text{DIN} + N_{\text{org}}$; $P_{\text{tot}} = \text{DIP} + P_{\text{org}}$), dissolved organic carbon (C_{org}), chlorophyll "a" (Chl-a), humic substances (Hum), overall salt composition parameters (Cl^- , SO_4^{2-} , Na^+ , K^+ , Ca^{2+} , Mg^{2+}), isotopic composition of the water ($\delta^{18}\text{O}$ and δD), and dissolved oxygen (DO). Based on the DO, the value of the apparent oxygen utilization (AOU) was calculated:

$$\text{AOU} = \text{DO}_{\text{equilibrium}} - \text{DO}_{\text{measured}} \quad (1)$$

Five-liter Niskin bottles were used for water sampling. Water samples were taken from the surface (depth of 0–0.5 m) and near-bottom (0.3–0.7 m from the bottom) water layers of up to 27 m depth. On the day of sampling, Chl-a samples were filtered and the pH, TA, DO, and concentration of nutrients in mineral form were measured. Salinity, N_{tot} and P_{tot} , macro-components, and stable isotopes were analyzed in the Hydrochemistry Laboratory of POI FEB RAS after the expedition.

An RBR maestro multi-channel logger (RBR Ltd., Ottawa, ON, Canada), 8 Hz sampling rate, was used for profiling the water. The following properties were measured: pressure, temperature, electrical conductivity, photosynthetically active radiation (PAR), Chl-a; chromophoric OM, DO, and turbidity.

Bottom sediments were sampled in each of the bays (Figure 1) using a one-meter-long gravity tubular sampler during the course of the winter expedition from 12 to 16 December 2022. The obtained cores were delivered to the shipboard laboratory, where pH was measured in different layers of the sediment at 10 cm intervals. After that, each layer of bottom sediment was stored at minus 80 °C. One month later, the bottom sediment was defrosted in the laboratory of POI FEB RAS over 12 h at +5 °C and then dewatered with a press to obtain pore water. The pore water was subjected to chemical analysis immediately after pressing. This paper presents the following characteristics of the pore waters obtained from the top layers of the 0–10 cm thick sediments: pH, TA, pCO_2 , DIC, NH_4^+ , DIP, DSi, N_{tot} , P_{tot} , C_{org} , Hum, Chl-a, and macro-component composition.

2.3. Laboratory Analysis

A potentiometric method was applied to determine the pH of the water. The pH was measured at 10 °C using a cell without a liquid junction [43] and reported on the total hydrogen ion concentration scale [44]. The precision of the pH measurements was about ± 0.004 pH units. TA analysis was carried out through direct colorimetric titration with hydrochloric acid in an open cell, according to the Bruevich method [45]. TA measurements were performed with a precision of ± 3 $\mu\text{mol}/\text{kg}$, with the accuracy set by calibration against certified reference materials. The pCO_2 , $\text{pH}_{\text{in situ}}$, and DIC were calculated from the measured pH and TA using a well-known procedure [19].

The concentration of NH_4^+ was determined using the indophenols method. The concentrations of NO_2^- , NO_3^- , DSi , and DIP were measured using standard colorimetric methods. Details of the methods used for the nutrient analyzes are given in Grasshoff et al. [46]. The detection limit was 0.01 $\mu\text{mol/L}$ for the phosphate and nitrite, and 0.02 $\mu\text{mol/L}$ for silicate. The concentration of N_{tot} and P_{tot} was determined using “Skalar San++” analyzer (Skalar, Breda, Netherlands).

Macro-ion concentrations were measured using the ion exchange chromatography method using a Shimadzu LC-20A chromatograph (Shimadzu, Kyoto, Japan). The alkalinity value was assumed as the hydrocarbonate ion (HCO_3^-) concentration. The total analytical error of the macro-ion determination was evaluated using NICB (normalized inorganic charge balance) values:

$$\text{NICB (\%)} = (\text{TZ}^+ - \text{TZ}^-) / \text{TZ}^+ \times 100 \quad (2)$$

where TZ^+ ($\mu\text{eq/kg}$) = $[\text{Na}^+] + [\text{K}^+] + 2[\text{Ca}^{2+}] + 2[\text{Mg}^{2+}]$ and TZ^- ($\mu\text{eq/kg}$) = $2[\text{SO}_4^{2-}] + [\text{Cl}^-] + [\text{HCO}_3^-]$. The mean value of NICB was $2.9 \pm 1.6\%$ for all fresh waters analyzed in this study and $0.48 \pm 0.15\%$ for the saline marine waters.

Measurements of isotopes of $\delta^{18}\text{O}$ and δD in water were conducted with a Picarro L-2130-I analyzer (Picarro, Santa Clara, CA, USA). The calculation of $\delta^{18}\text{O}$ and δD values was based on the recalculation of the detector signal using the standard software “CRDS Data Viewer Picarro”. The relationship between δD and $\delta^{18}\text{O}$ was defined as the meteoric water line. Inter-laboratory reference samples were used as standards pegged to the V-SMOW-2 standard. The reproducibility of the measurements was 0.1‰ for $\delta^{18}\text{O}$ and 0.5‰ for δD .

Preparation of a water sample for Chl-a determination considered the following: 1 L water sample was filtered through 2 μm and extracted from the filters in a 90% acetone solution. The optical density of light absorption in the extracts was measured on a Shimadzu UV-3600 spectrophotometer (Shimadzu, Kyoto, Japan). Before measuring the pheophytin content, the extract was pre-acidified with 2–3 drops of a hydrochloric acid solution in acetone.

DO samples were analyzed using the Winkler titration method, an automated oxygen titrator with a Brinkman Dosimat burette, and photometric end-point detection, providing an accuracy of the measurements of 0.5 to 1%.

The software used for statistical analyses was MS Excel 2019. The spatial distribution maps were developed using the program Surfer 9 of Golden Software 9.1.352 ((Golden Software LLC) Golden, CO, USA).

3. Results

3.1. Characteristics of End Members

3.1.1. Salt and Isotopic Composition

The chemical characteristics of the Avacha R. and Vilyucha R. waters and melted waters (waterfall) are presented in Table 2. The waters studied were nonsaline in flood periods in July and in the low water period in December 2022. TDS = 40 mg/L in melted waters; 69 and 73 mg/L in Avacha R., 37 and 123 mg/L in Vilyucha R. in July and December, respectively.

The fresh waters in July 2022, and in Avacha R. in December 2022, were of a hydrocarbonate-calcium type, which is typical of the rivers in humid climate regions. The macro-ion concentrations in the river waters of the study area were consistent with mean global concentrations [47]. An exception was sulfate ions, with their concentrations in Vilyucha R. and particularly in Avacha R. being increased compared with global values for rivers.

Possibly, the increased of SO_4^{2-} concentrations observed in the river waters of Kamchatka are a natural regional baseline characteristic of river drainage basins in a volcanic area. It is likely that the source of sulfate ions is volcanic aerosol of ash/gas clouds, which include sulfur oxides producing sulfuric acid when in contact with atmospheric moisture [48].

Table 2. Water characteristics. pH—pH_{in situ} on the total hydrogen ion concentration scale [44], Chl-a—in water (µg/L), in bottom sediments (µg/g dry residue). PW—pore water. SW—sea water. Pore water characteristics are shown for the sediment layer 0–10 cm. Highlighted in blue are the river water characteristics in winter.

	Cl ⁻	SO ₄ ²⁻	Na	K ⁺ mmol/kg	Ca ²⁺	Mg ²⁺	δ ¹⁸ O ‰	δD ‰
Vilyucha River	0.082	0.053	0.150	0.014	0.138	0.042	-13.78	-96.83
	1.155	0.125	1.143	0.0437	0.213	0.165	-13.79	-96.07
Avacha River	0.101	0.151	0.219	0.028	0.250	0.108	-16.23	-118.28
	0.140	0.144	0.264	0.023	0.262	0.106	-15.54	-111.16
Waterfall	0.052	0.023	0.085	0.003	0.186	0.039	-13.37	-97.66
SW upper layer	510.610	26.4	439.5	9.46	9.45	49.54	-1.08	-8.58
PW Vilyucha Bay	554.4	27.68	482.6	11.805	9.99	53.03		
PW Avacha Bay	536.2	24.812	464.1	11.058	9.772	50.657		
	DIP	DSi	NO ₂	NO ₃ µmol/L	NH ₄	DIN	Total P	Total N
Vilyucha River	0.47	247.28	0.03	24.29	0.36	24.68	0.7	27.28
	0.8	227.01	0.07	31.53	2.41	34.01	1.1	40.05
Avacha River	0.74	193.03	0.10	19.51	1.84	21.45	0.77	20.68
	0.73	300.4	0.11	43.01	1.44	44.56	1.02	48.74
Waterfall	0.11	108.68	0.03	36.37	0.28	36.68	0.11	39.33
SW upper layer	0.15	18.77	0.02	0.07	0.28	0.37	0.77	14.4
PW Vilyucha Bay	40.71	440.5	1.3	-	69.1	-	83.45	3239
PW Avacha Bay	92.08	565.72	0.46	-	-	-	147.65	1868
	pH	TA mmol/kg	pCO ₂ µatm	DIC mmol/kg	Corg mgC/L	Hum mgC/L	Chl-a	O ₂ µmol/kg
Vilyucha River	8.95	0.31	15.8	0.30	0.64	0.44	0.18	391.7
	7.74	0.49	385	0.52	0.54		0.60	
Avacha River	-	0.532	-	-	-	-	-	-
	-	0.56	-	-	-	-	-	-
Waterfall	8.69	0.41	39.9	0.40	0.37	-	-	-
SW upper layer	8.33	2.0	167.9	1.72	1.1	0.32	3.01	363.4
PW Vilyucha Bay	7.32	3.7	3187	3.38	210.9	29.0	15.98	-
PW Avacha Bay	7.23	6.2	7106	6.26	124.2	20.03	16.12	-

The macro-component composition of the pore waters in the sediment layer 0–10 cm generally coincided with that of the sea waters (Table 2).

The isotopic composition of Vilyucha R. waters in summer and winter seasons was virtually the same and close to the composition of melted water from the waterfall. However, the isotopic composition of the Avacha R. waters was significantly lower compared with the Vilyucha R. waters (Table 2).

3.1.2. Nutrients

In summer, the largest concentration of DIN = 36.68 µmol/L dominated by ions NO₃⁻ = 36.37 µmol/L was found in melted water from the waterfall. The maximum concentration of DSi = 247 µmol/L and increased DIN and NO₃⁻ concentrations (24.68 and 24.29 µmol/L respectively) were registered in Vilyucha R. waters. The P_{tot} and N_{tot} concentrations were close to the DIP and DIN concentrations; i.e., nutrients were found primarily in mineral form. A significant increase in DIP to 5.47 µmol/L was registered in the near-bottom layers of Avachinskaya Bay.

Table 2 shows that the summer molar ratio of DIN/DIP was determined as 52.5 and 29 for Vilyucha R. and Avacha R., respectively, while the DIN/DIP of melted water from the waterfall was 333. DIN/DIP = 2.5 for sea water in the surface layer and 6.6 in near-bottom layers. DIN/DIP = 1.72 for the pore waters in Vilyuchinskaya Bay.

In the summer season, very low $p\text{CO}_2$ values were registered in Vilyucha R.— $15.8 \mu\text{atm}$ and in the waterfall— $39.9 \mu\text{atm}$ and the pH value was high—about 9. In the winter season, the carbonate system parameters greatly changed in the river: the $p\text{CO}_2$ value increased to $385 \mu\text{atm}$ and the pH value reduced to 7.74. At the same time, the C_{org} , Hum, Chl-a, and O_2 concentrations did not undergo any significant fluctuations between summer and winter data.

In the pore water, the pH varied in the range of 7.23–7.44. The TA, $p\text{CO}_2$ DIC values in the sediments of Avachinskaya Bay were nearly twice as high as in Vilyuchinskaya Bay. At the same time, the C_{org} concentration in the pore waters was highest in Vilyuchinskaya Bay— 210 mgC/L .

3.2. Spatial Distribution of Characteristics Obtained by Profiling

The Vilyucha R. has a relatively low flow rate, and because of that, its fresh water plume with salinity under 24 extends to a distance of 3.5 km, only occupying the space above the seabed depression up to 20 m deep (Figure 3). Low temperatures of the surface layer waters (about $4 \text{ }^\circ\text{C}$) were only registered in the immediate vicinity of the river, at depths of about 1 m. In general, across the transect, the surface and near-bottom water layers had temperatures of about 13 and $2\text{--}2.5 \text{ }^\circ\text{C}$, respectively (Figure 3). The near-surface water layer was oversaturated with oxygen compared with the atmosphere (115–120%). An increase in Chl-a to $5\text{--}9 \mu\text{g/L}$ was observed in the near-surface water layer 5–10 m thick. The water at near-bottom levels, particularly above the seabed depression, was under-saturated with oxygen (Figure 3).

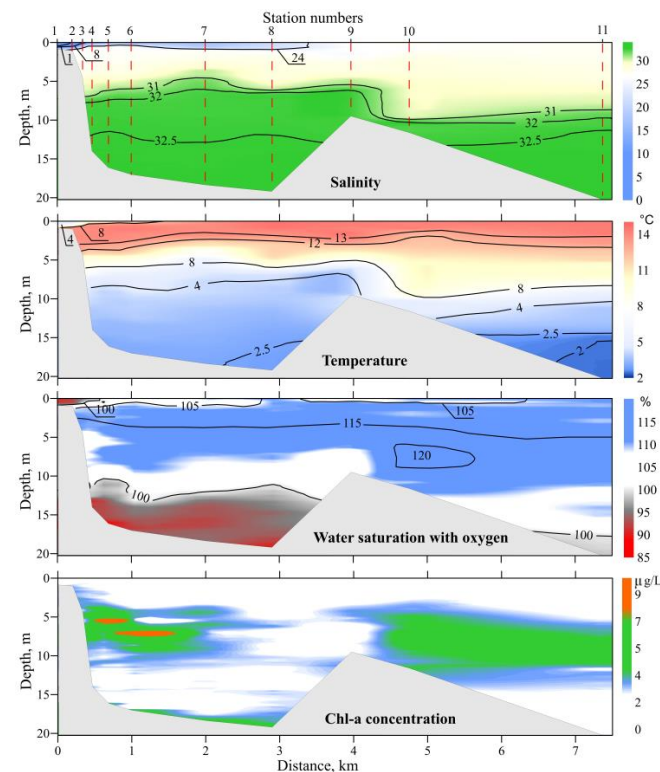


Figure 3. Variability of water characteristics across the longitudinal profile of the estuary of Vilyucha R. and Vilyuchinskaya Bay. (Left side)—river, (right side)—sea. The distance from the river mouth cross line is shown on the X axis (St. 1).

Observations were made at locations in the research grid in Avachinskaya Bay at water depths of 20–27 m (Figure 1), which is about 10 m more than the depth at the cross line of the narrow entry to the Bay. Figure 4 demonstrates a typical distribution of the characteristics in Avachinskaya Bay. In this water basin, a freshened surface layer was

observed with salinity within 20–25, with a temperature of about 12 °C and an increased Chl-a content of about 10 µg/L. Water saturation reached its maximum of 143% in the near-surface water layer at the 4 m level at the station located closest to the Avacha R. The water saturation declined to its minimum of 45% in near-bottom water layers in both the eastern and western parts of the bay.

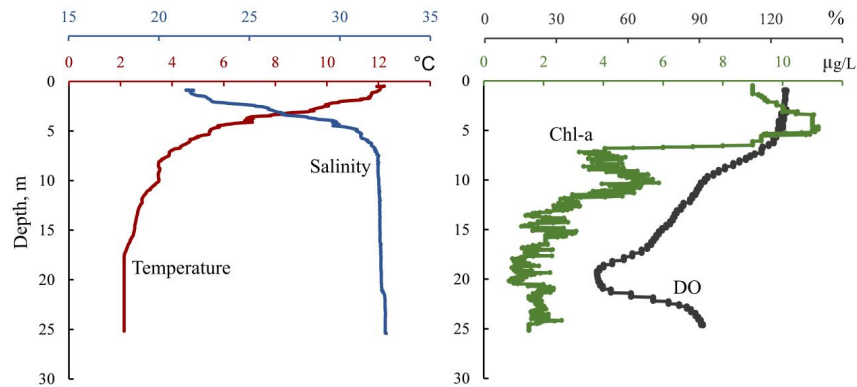


Figure 4. Vertical distribution of salinity, temperature, Chl-a, DO in Avachinskaya Bay in the vicinity of the bottom sediment sampling station on 5 July 2022.

3.3. Parameters of the Carbonate System, Chl-a and AOU in the Surface and Near-Bottom Water Layers

Extremely low pCO₂ values of 15.8 and 39.9 µatm were obtained for Vilyucha R. and the waterfall on the coast of Vilyuchinskaya Bay. An excess of pCO₂ compared with its atmospheric value was observed for the surface waters at a salinity of up to 2.1 in Vilyuchinskaya Bay and for near-bottom waters at a salinity of more than 32 in Avachinskaya Bay (Figure 5).

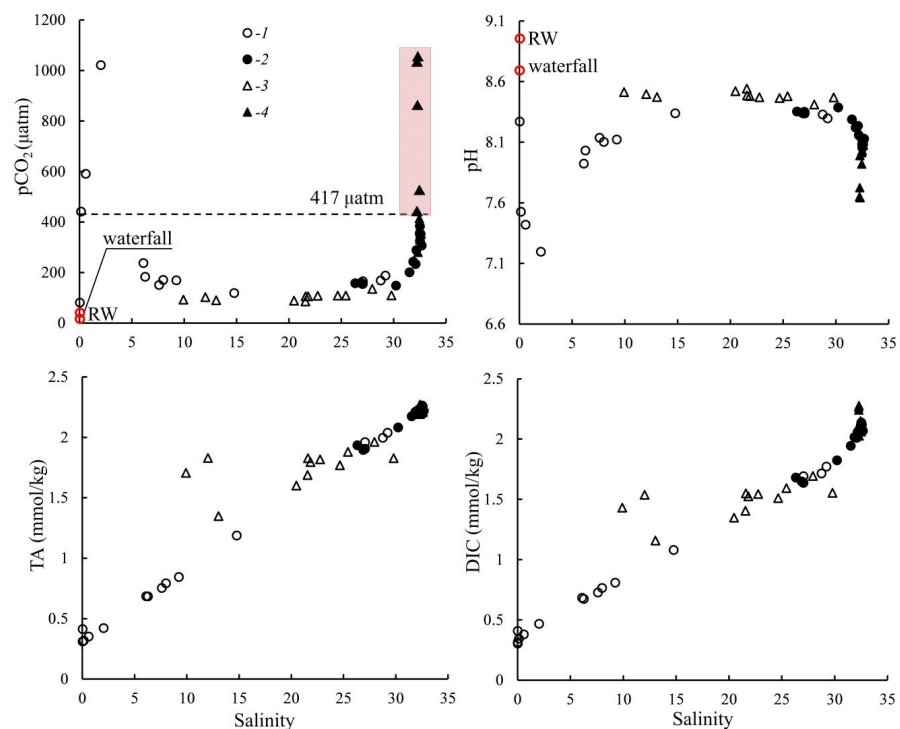


Figure 5. Carbonate system parameters vs. water salinity. 1, 2—surface and near-bottom water layers in Vilyuchinskaya Bay; 3, 4—surface and near-bottom water layers in Avachinskaya Bay. Red colors indicate the pCO₂ growth in near-bottom waters layers. RW = river waters of Vilyucha R.

The pH values were mostly reversely proportional to the pCO₂ values. The maximum pH value of 8.95 was registered in Vilyucha R. and rapidly declined as the river waters mixed with marine waters at a salinity of up to 2.1. The minimum pH value of 7.64 was observed in the near-bottom layer of the Avachinskaya Bay waters (Figure 5).

The distribution of TA and DIC generally had a similar profile and was governed by the river and marine water mixing processes. However, the DIC distribution showed additional carbon in the near-bottom waters of Avachinskaya Bay (Figure 5). Carbon addition led to an increased TA/DIC ratio, as seen in Figure 6.

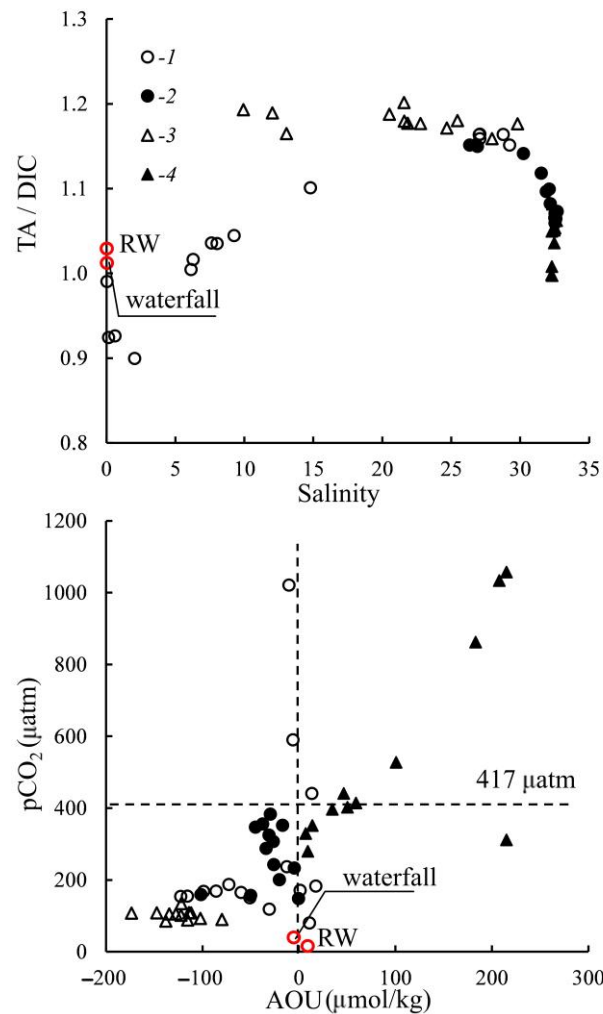


Figure 6. Ratio of carbonate system parameters (TA/DIC) vs. salinity and pCO₂ vs. AOU. 1, 2—surface and near-bottom water layers in Vilyuchinskaya Bay; 3, 4—surface and near-bottom water layers in Avachinskaya Bay. RW = river waters of Vilyucha R. Dotted lines show equilibrium values.

Based on the pCO₂ vs. AOU, two features can be singled out (Figure 6): the first features is characterized by the simultaneous growth of pCO₂ from 107 μatm and AOU from minus 173 μmol/kg to 1057 μatm and 215 μmol/kg, respectively; the second feature is characterized by an abrupt increase in pCO₂ from 15.8 to 1.020 μatm with a constant AOU value. The AOU was primarily in the negative range in Vilyuchinskaya Bay, including its near-bottom waters. In Avachinskaya Bay, the AOU varied from −173.4 μmol/kg in the surface layers to 207.6 μmol/kg in the near-bottom waters, which is indicative of surface water oversaturation and near-bottom water under-saturation with oxygen.

3.4. Nutrients in the Surface and Near-Bottom Water Layers

For the water basins under consideration, an overall reduction in the content of nutrients in the surface water layer from the river toward the sea and its significant increase in near-bottom water layers was observed (Figure 7). High DIN/DIP ratios were obtained for the estuary of Vilyucha R. and low ones were obtained for the estuary of Avacha R. at a water salinity of up to about 15, and high DSi/DIP ratios were obtained in the river and estuary waters of both water basins (Figure 7). The DSi/DIN ratio was low in the river and near-bottom marine waters—down to 3 and 1.3, respectively, and high in the surface layer of Avachinskaya Bay and seaward part of Vilyuchinskaya Bay at a salinity of more than 26 (Figure 7).

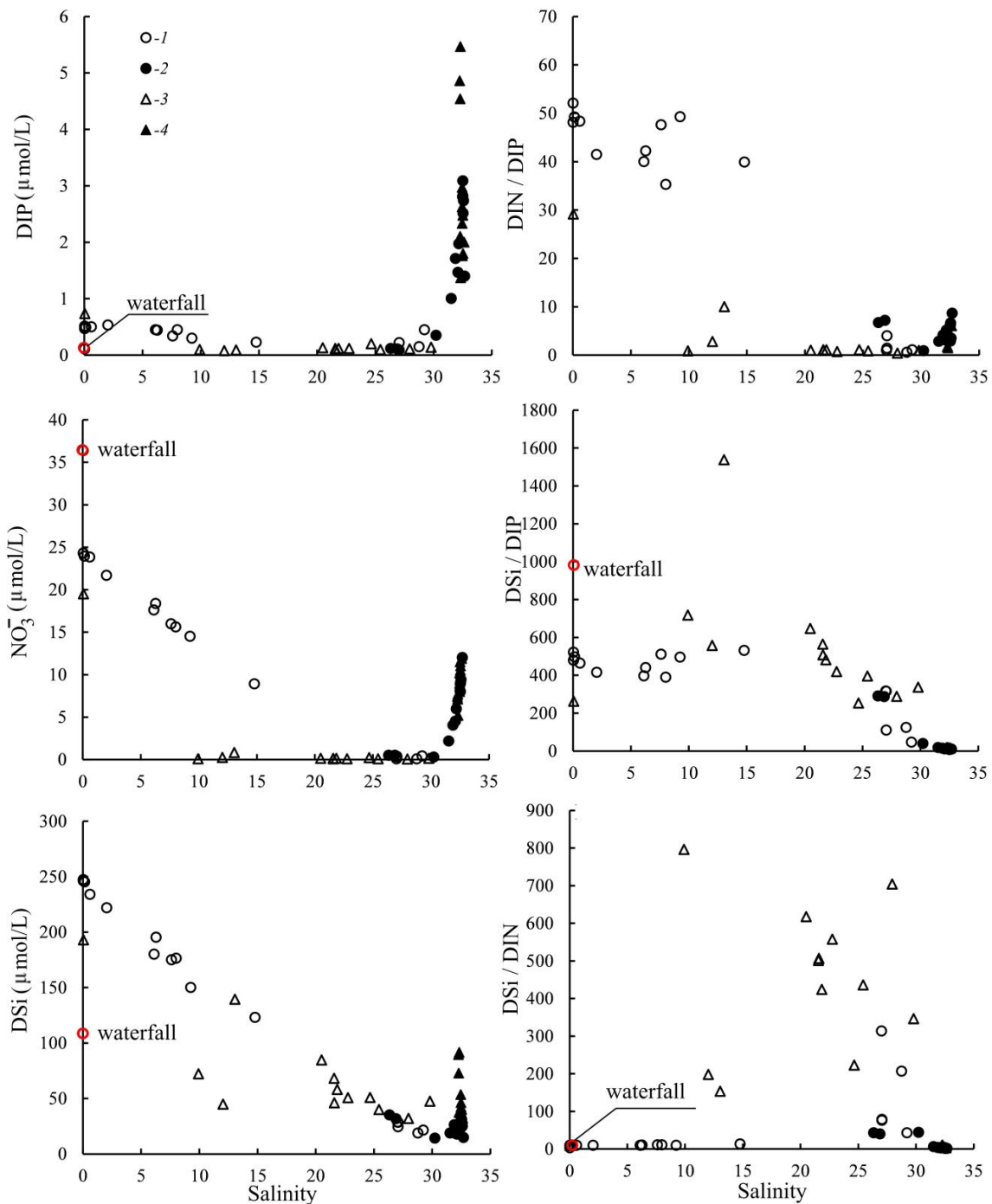


Figure 7. Nutrients and their ratios. 1, 2—surface and near-bottom water layers in Vilyuchinskaya Bay; 3, 4—surface and near-bottom water layers in Avachinskaya Bay.

4. Discussion

The direction and intensity of the OM production/destruction balance is governed by the PAR intensity and supply of nutrients, as well as by the zooplankton grazing rate and viral lysis of phytoplankton cells. Although bottom sediments were sampled in December, we discuss these results together with other results obtained in July, as the water temperatures in the core sampling locations differed insignificantly between the two expeditions—less than 0.5 °C. That is why an assumption was made that the potential hydrological effects insignificantly affected the geochemical processes in the sediments at the turn of the seasons.

4.1. River Feeding Sources and Nutrient Fluxes with River Runoff

The Vilyucha and Avacha Rivers were different in their isotopic composition of $\delta^{18}\text{O}$ and δD (Table 2), which is indicative of the different inputs provided from the feeding sources of these rivers by rainwater, melted water from highlands, and from river valleys. The isotopic composition of snow and ice on volcanoes largely depends on the altitude above sea level [49]. In the area under consideration, $\delta\text{D} = -115\text{‰}$ and $\delta^{18}\text{O} = -15\text{‰}$ at altitudes of about 2000 m above sea level [50]. The feeding sources of Vilyucha R. and of the waterfall are snow and ice, which are found in roughly equal measure, as their isotopic compositions coincide (Table 2). The Avacha R. is fed by melted water from the largest volcanoes—Koryakskiy and Avachinskiy. This probably explains the lighter $\delta^{18}\text{O}$ and δD composition in its water, close to that of snow and ice at the altitude of more than 2000 m above sea level [50]. In the relatively large watershed of Avacha R., rainwater accumulates during the spring–summer season, contrarily to the small watershed of Vilyucha R., where rainwater rapidly runs down the watershed for several days after rainfall. The presence of rainwater makes the isotopic composition of Avacha R. lighter compared with Vilyucha R.

The Vilyucha R., Avacha R., and melted waters of the waterfall had relatively high NO_3^- concentrations (Table 2). The obtained concentrations are comparable with the NO_3^- concentrations in anthropogenically polluted rivers; for example, in the Razdolnaya River flowing across an urbanized area in China and Russia (NO_3^- range is 10–30 $\mu\text{mol/L}$ in the high water period and up to 300 $\mu\text{mol/L}$ in the low water period) [51]; in Japanese rivers subjected to anthropogenic nitrate flux (NO_3^- range is 18–55 $\mu\text{mol/L}$) [52]; and in small rivers in China with anthropogenic effluents (NO_3^- range is 15–368 $\mu\text{mol/L}$) [53]. At the same time, the NO_3^- concentrations are much lower (0.02–0.37 $\mu\text{mol/L}$ in the high water period) in the Sea of Okhotsk rivers not exposed to anthropogenic loads and volcanic activities [54].

The flux of nutrients supplied by the Vilyucha and Avacha Rivers to the receiving water basins was calculated using the following ratio:

$$F_i = Q \cdot C_i \quad (3)$$

where F_i —flux of “I” substance; Q —water discharge of the river; and C_i —“i” substance concentration in river waters. The estimated nutrient fluxes are presented in Table 3. Table 3 also presents data for nutrient flux with runoff for the taiga river Usalgin (the Sea of Okhotsk). The FDIN in Avacha R. is much higher than the FDIN in Usalgin R. The summer nutrient flux of the Vilyucha and Avacha River runoff was roughly 2–3 times larger than the winter flux (Table 3), due to the increased discharge into these rivers in the high water period.

The increased NO_3^- concentration and accordingly relatively high FDIN may have been caused by two factors. First, the snow and ice become enriched with nutrients during volcanic eruptions [55,56], and the largest amounts of tephra were observed in the vicinity of volcano summits in the study area [57]. Second, it should be anticipated that the melted water flowing across volcanic soils of the study area [41] will be additionally enriched with nutrients and ultimately deliver them to the river. Another additional, although probably insignificant, nutrient flow may be related to the fact that the hydrothermal

systems in the watersheds have numerous hot springs issuing steam jets enriched with nitrogen and phosphorus [58]. Due to steam condensation, these substances accumulate in the snow cover during winter and are supplied to rivers during snow melting. However, this region’s thermal waters, sampled from numerous wells, have an isotopic composition that is heavier compared with melted waters, due to $\delta^{18}\text{O}$ and δD isotopes [58], their flow rate is incomparably lower than that of rivers, and they are unlikely to have any significant influence on the chemical composition of the Vilyucha and Avacha Rivers in summer.

Table 3. Daily flux (tons/day) with rivers discharge (m^3/s), dissolved inorganic phosphorus $FDIP$, nitrogen $FDIN$, silicates $FDSi$; total phosphorus FP_{tot} and nitrogen FN_{tot} . Blue color highlights flux in the winter season.

River	Discharge	$FDIP$	FP_{tot}	$FDSi$	$FDIN$	FN_{tot}
Vilyucha	28	0.035	0.052	16.75	0.83	0.92
	7	0.015	0.021	4.69	0.29	0.29
Avacha	288	0.571	0.59	134.49	7.2	7.47
	77	0.151	0.21	55.96	4.15	4.15
Waterfall	0.3	0.00009	0.00009	0.079	0.013	0.014

4.2. OM Production/Destruction Balance

The OM production/destruction balance is largely governed by the thickness of the photic layer, which was 12–18 m in Vilyuchinskaya Bay and almost everywhere reached the bottom of this water basin. In Vilyucha R., transparent water was observed with a current velocity of about 1.5 m/s. The photic layer thickness in the Avachinskaya Bay was somewhat smaller (about 9 m) because of a significantly greater suspended matter flow in the runoff of the Avacha R. The water depth in Avachinskaya Bay reached 27 m in locations where the water samples were taken.

The amount of primary production in Avachinskaya Bay, according to [59], is reduced in July compared with other summer months, due to a decreased photic layer thickness and is $0.89 \text{ gCm}^{-2} \text{ day}^{-1}$. According to these data, the amount of primary production for the whole Avachinskaya Bay with a square area of $254 \times 10^6 \text{ m}^{-2}$ is about 226 tons day^{-1} . If adopt this amount of primary production per square area unit for Vilyuchinskaya Bay, it would be about $12.9 \text{ tons day}^{-1}$ for this Bay’s basin with a square area of $14.5 \times 10^6 \text{ m}^{-2}$. The obtained C fluxes from the atmosphere to the water for Vilyuchinskaya and Avachinskaya Bays were 3.6 and 132 tons C day^{-1} , respectively, which is less than the primary production values of 12.9 and 226 tons C day^{-1} .

The inverse relation between the $p\text{CO}_2$ and AOU in the mixing zone (Figure 6) shows that CO_2 content is mainly controlled by the OM production/destruction balance. The rate of O_2 consumption in the case of aerobic bacterial oxidation is governed by the OM concentration in the water. That is why, when the $p\text{CO}_2$ values are high, the highest AOU value is observed in the bay’s near-bottom layers, where the PAR intensity is decreased.

The dominance of aerobic oxidation in the near-bottom layers of the water basins results in the growth of AOU, $p\text{CO}_2$, DIC, DIN, DIP, but a decreased value of $\text{pH}_{\text{in situ}}$, and the dominance of micro-algae photosynthesis in the surface layers results in the opposite situation (Figures 5–7). The combination of a relatively high nutrient flux with river runoff and low suspended matter concentration in the river waters results in a relatively high primary production level in the water basins, contrary to urbanized estuaries with high water turbidity and small photic layer thickness.

4.3. Potential Response of the Estuary Ecosystem to Nutrient Flux and Possible Cases of Red Tides

In general, the obtained data (Figures 4 and 7) show that the Vilyuchinskaya and Avachinskaya Bays are oligotrophic through a complex of parameters [60]. To a certain degree, Avachinskaya Bay can be considered an eutrophicated basin, because it is subjected to seasonal hypoxia, with the DO concentrations in the near-bottom waters dropping to less than 2 mL/L [36,37]. The seasonal hypoxia observed in the Avachinskaya Bay is largely

related to its specific morphometric characteristics—a narrow shallow-water threshold at the entrance to the Bay, which prevents its water exchange with the waters of the Pacific Ocean. The photic layer thickness in the Vilyuchinskaya Bay at the time of our expedition reached the seabed, while the photic layer in Avachinskaya Bay did not exceed 15 m at this basin's depth of 27 m. The seasonal hypoxia in the Avachinskaya Bay is related to the increased inflow of nutrients in the spring–summer period, the peak of which occurs roughly in late June—the time of the highest flow rate in the Avacha R. Furthermore, the maximum river runoff in this period leads to the development of density stability and a reduction in photic layer thickness in Avachinskaya Bay, similar to the processes occurring in eutrophicated coastal basins [8,60]. However, in this case, the main source of nutrients is volcanism enriching the snow cover with nitrogen and phosphorus compounds, which was confirmed by their relatively high concentration in the Vilyucha R. compared with Avacha R., which has no anthropogenic sources of nutrients.

Due to anthropogenic loads and related phytoplankton blooms, nutrient fluxes from river runoff are widely discussed [2,6,7]. Absolute nutrient concentrations play a central role in the dynamic of an ecosystem, but the DIN/DIP ratio also affects some ecological trends and processes [61]. According to the latest studies [14,15] and previous articles [62], dinoflagellates, including potentially toxic species, dominate in the case of a significant growth in DIN/DIP ratios. This is related to the capability of dinoflagellates to use different forms of P in their competition with diatoms [13,16]. The maximum values of nutrient flux from river runoff being registered in summer may partly explain the harmful blooms frequently observed in the study area over the last 50 years and normally occurring in August–October [38]. The most publicized case of toxic dinoflagellate *Karenia* (Dinophyceae) blooming on the coast of the Avacha Bay occurred in September 2020, when a related Instagram post gained more than one million views [39].

In general, the DIN/DIP ratio obtained for sea water is typical of this area of the Pacific Ocean, as it is 2.5 on the surface, about 10 at the depth of 50 m, and gently increases to 13–14 as the depth increases in the intermediate and deep waters of the Pacific Ocean [63]. However, the DIN/DIP ratios in river and melted waters were increased (Table 2, Figure 7).

The pore waters in the sediments of the Vilyuchinskaya and Avachinskaya Bays contain high C_{org} and N_{tot} concentrations (Table 2). DIP is normally adsorbed in sediments but redox potential greatly affects the P dissolution in sediments [64]. In the water column and bottom sediments, phosphorus adsorption/desorption in the course of ion exchange with Fe compounds may significantly influence the DIP concentrations [65,66]. Therefore, Fe compounds act as DIP source or scavenger in the water column and bottom sediments. This can explain the high DIP concentrations in the pore waters of the top layer of the precipitate (Table 2). Nutrient flux was not calculated from the bottom sediments in this paper, because the key findings apply to July and precipitate studies were carried out in December. However, the existence of high Chl-a concentrations in bottom sediments (Table 2) is evidence of intensive exchange between pore waters and near-bottom waters.

Hence, river runoff intensification will be accompanied by an increased DIN/DIP ratio, due to an increased DIN flux, and the water exchange at the water/bottom boundary is accompanied by its reduction, due to an additional DIP flux. The supply of intermediate Pacific waters due to upwelling results in equal DIN/DIP ratios within the range of 10–14.

If we take the conclusions made in previous studies [11–16] on interrelation of red tides and DIN/DIP ratio variation toward higher DIN as a basis, the coastal runoff in the area of Vilyuchinskaya and Avachinskaya Bays can be considered one of the factors capable of triggering dinoflagellate development after the high water peak in mid-summer. It is known that different types of ash contribute different ratios of DIN and DIP fluxes, and there are differences in ash, depending on the distance from active volcanoes [67]. Additionally, the DIN flux and stimulation of phytoplankton blooms may result from groundwater discharges [3] and porewater exchange [68], as occurs in other regions. In this case, this may be applicable to Kamchatka, since volcanic rocks have a high permeability to groundwater, which is enriched with DIN and DIP during water–soil interactions.

The next stage of this work will be to find possible correlations between phytoplankton blooms, including red tides, and the intensity of volcanism and submarine groundwater discharge in the coastal areas of Kamchatka.

5. Conclusions

Studies of nutrient flux with river runoff often focus on anthropogenic sources. In this paper, the nutrient flux discussed was primarily that of mineral nitrogen and phosphorus, formed by a natural source—the volcanism in the Kamchatka Peninsula. The maximum flux of nutrients resulting from the runoff of the Vilyucha and Avacha Rivers occurs at the peak of the high water period in June–early July, i.e., at the time of volcanic ash-enriched snow melt in highlands. As a result of this, phytoplankton blooming occurs, and surface waters become oversaturated with oxygen and undersaturated with CO₂. The obtained results proved that any studies of nutrient flux with river runoff in this region should make provision for temperature conditions, snow melt intensity, and preceding ash falls in the winter season in the river drainage basins. Accordingly, potential climate changes in the future may be accompanied by varying levels of nutrient and organic matter flux with river runoff to coastal/marine basins in this region.

Author Contributions: P.S.: Writing—Original draft, Conceptualization, Methodology, Formal analysis, Investigation, Funding acquisition. G.P.: Writing—review and editing, Investigation, Formal analysis. V.L.: review and editing, Funding acquisition Investigation Y.B.: Methodology, Formal analysis, Investigation. S.K.: Methodology, Formal analysis, Investigation. S.S.: Methodology, Formal analysis, Investigation. M.S.: Methodology, Formal analysis, Investigation. E.S.: Methodology, Formal analysis, Investigation P.T. (Petr Tishchenko): Methodology, Formal analysis, Investigation. E.T.: Methodology, Formal analysis, Investigation. O.U.: Methodology, Formal analysis, Investigation. P.T. (Pavel Tishchenko): Writing—review and editing, Investigation, Conceptualization, Supervision, Funding acquisition. All authors have read and agreed to the published version of the manuscript.

Funding: This work was supported by the Comprehensive interdepartmental program Environmental Safety of Kamchatka (NIOKTR 122110100002-8) and Program of fundamental research of the Russian Academy of Sciences for 2021–2023, projects 0211-2021-0008 and 0211-2021-0014.

Institutional Review Board Statement: Not applicable.

Informed Consent Statement: Not applicable.

Data Availability Statement: Any datasets not included in the published work are available upon reasonable request from the corresponding author; however, all data produced or analyzed during this investigation are contained in the article.

Acknowledgments: The support of the scientific groups and crews of R/Vs Gagarinskiy and Akademik Oparin is greatly appreciated.

Conflicts of Interest: The authors declare no conflict of interest.

References

1. Nixon, S.F. Coastal marine eutrophication: A definition, social causes, and future concerns. *Ophelia* **1995**, *41*, 199–219. [[CrossRef](#)]
2. Andersen, J.H.; Schlüter, L.; Ertebjerg, G. Coastal eutrophication: Recent developments in definitions and implications for monitoring strategies. *J. Plan. Res.* **2006**, *28*, 621–628. [[CrossRef](#)]
3. Aoki, K.; Shimizu, Y.; Yamamoto, T.; Yokouchi, K.; Kishi, K.; Akada, H.; Kurogi, H. Estimation of inward nutrient flux from offshore into semi-enclosed sea (Tokyo Bay, Japan) based on in-situ data. *Estuar. Coast. Shelf Sci.* **2022**, *274*, 107930. [[CrossRef](#)]
4. Howarth, R.W. Coastal nitrogen pollution: A review of sources and trends globally and regionally. *Harmful Algae* **2008**, *8*, 14–20. [[CrossRef](#)]
5. Anderson, D.M.; Cembella, A.D.; Hallegraeff, G.M. Progress in understanding harmful algal blooms: Paradigm shifts and new technologies for research, monitoring, and management. *Annu. Rev. Mar. Sci.* **2012**, *4*, 143–176. [[CrossRef](#)]
6. Glibert, P.M.; Anderson, D.M.; Gentien, P.; Granéli, E.; Sellner, K.G. The global, complex phenomena of harmful algal blooms. *Oceanography* **2005**, *18*, 136–147. [[CrossRef](#)]
7. Glibert, P.M. Harmful algae at the complex nexus of eutrophication and climate change. *Harmful Algae* **2020**, *91*, 101583. [[CrossRef](#)] [[PubMed](#)]

8. Zhang, J.; Gilbert, D.; Gooday, A.J.; Levin, L.; Naqvi, S.W.A.; Middelburg, J.J.; Scranton, M.; Ekau, W.; Peña, A.; Dewitte, B.; et al. Natural and human hypoxia and consequences for coastal areas: Synthesis and future development. *Biogeosciences* **2010**, *7*, 1443–1467. [[CrossRef](#)]
9. Schmodtko, S.; Stramma, L.; Visbeck, M. Decline in global oceanic oxygen content during the past five decades. *Nature* **2017**, *542*, 335–339. [[CrossRef](#)]
10. Breitburg, D.; Levin, L.A.; Oschlies, A.; Gregoire, M.; Chavez, F.P.; Conley, D.J.; Garçon, V.; Gilbert, D.; Gutierrez, D.; Isensee, K.; et al. Declining oxygen in the global and coastal waters. *Science* **2018**, *359*, eaam7240. [[CrossRef](#)]
11. Hodgkiss, I.; Ho, K. *Are Changes in N: P Ratios in Coastal Waters the Key to Increased Red Tide Blooms?* Springer: Berlin/Heidelberg, Germany, 1997; pp. 141–147.
12. Paerl, H.W. Coastal eutrophication and harmful algal blooms: Importance of atmospheric deposition and groundwater as “new” nitrogen and other nutrient sources. *Limnol. Oceanogr.* **1997**, *42*, 1154–1165. [[CrossRef](#)]
13. Huang, K.; Zhuang, Y.; Wang, Z.; Ou, L.; Cen, J.; Lu, S.; Qi, Y. Bioavailability of Organic Phosphorus Compounds to the Harmful Dinoflagellate *Karenia mikimotoi*. *Microorganisms* **2021**, *9*, 1961. [[CrossRef](#)] [[PubMed](#)]
14. Zhang, Q.-C.; Wang, Y.-F.; Song, M.-J.; Wang, J.-X.; Ji, N.J.; Liu, C.; Kong, F.-Z.; Yan, T.; Yu, R.C. First record of a Takayama bloom in Haizhou Bay in response to dissolved organic nitrogen and phosphorus. *Mar. Poll. Bull.* **2022**, *178*, 113572. [[CrossRef](#)]
15. Medina, M.; Kaplan, D.; Milbrandt, E.C.; Tomasko, D.; Huffaker, R.; Angelini, C. Nitrogen-enriched discharges from a highly managed watershed intensify red tide (*Karenia brevis*) blooms in southwest Florida. *Sci. Total Environ.* **2022**, *827*, 154149. [[CrossRef](#)] [[PubMed](#)]
16. Shen, A.; Liu, H.; Xin, Q.; Hu, Q.; Wang, X.; Chen, J. Responses of Marine Diatom–Dinoflagellate Interspecific Competition to Different Phosphorus Sources. *J. Mar. Sci. Eng.* **2022**, *10*, 1972. [[CrossRef](#)]
17. Tréguer, P.J.; De La Rocha, C.L. The World Ocean silica cycle. *Ann. Rev. Mar. Sci.* **2013**, *5*, 477–501. [[CrossRef](#)]
18. Sarthou, G.; Timmermanns, K.R.; Blain, S.; Tréguer, P. Growth physiology and fate of diatoms in the ocean: A review. *J. Sea Res.* **2005**, *53*, 25–42. [[CrossRef](#)]
19. Dickson, A.G.; Sabine, C.L.; Christian, J.R. (Eds.) *Guide to Best Practices for Ocean CO₂ Measurements*; PICES Special Publication 3; PICES: Sidney, BC, Canada, 2007; 191p, Available online: <http://hdl.handle.net/11329/249> (accessed on 31 October 2022).
20. Symonds, R.B.; Reed, M.H.; Rose, W.I. Origin, speciation, and fluxes of trace-element gases at Augustine volcano, Alaska: Insights into magma degassing and fumarolic processes. *Geochim. Cosmochim. Acta* **1992**, *56*, 633–657. [[CrossRef](#)]
21. Li, Y.; Keppeler, H. Nitrogen speciation in mantle and crustal fluids. *Geochim. Cosmochim. Acta* **2014**, *129*, 13–32. [[CrossRef](#)]
22. Duggen, S.; Croot, P.; Schacht, U.; Hoffmann, L. Subduction zone volcanic ash can fertilize the surface ocean and stimulate phytoplankton growth: Evidence from biogeochemical experiments and satellite data. *Geophys. Res. Lett.* **2007**, *34*, L01612. [[CrossRef](#)]
23. Martin, J.H.; Coale, K.H.; Johnson, K.S.; Fitzwater, S.E.; Gordon, R.M.; Tanner, S.J.; Hunter, C.N.; Elrod, V.A.; Nowicki, J.L.; Coley, T.L.; et al. Testing the iron hypothesis in ecosystems of the equatorial Pacific Ocean. *Nature* **1994**, *371*, 123–129. [[CrossRef](#)]
24. Boyd, P.; Watson, A.; Law, C.; Abraham, E.; Trull, T.; Murdoch, R.; Bakker, D.; Bowie, A.; Buesseler, K.; Chang, H.; et al. A mesoscale phytoplankton bloom in the polar Southern Ocean stimulated by iron fertilization. *Nature* **2000**, *407*, 695–702. [[CrossRef](#)]
25. Frogner, P.; Gislason, S.R.; Oskarsson, N. Fertilizing potential of volcanic ash in ocean surface water. *Geology* **2001**, *29*, 487–490. [[CrossRef](#)]
26. Hoffmann, L.J.; Breitbarth, E.; Ardelan, M.V.; Duggen, S.; Olgun, N.; Hasselov, M.; Wangberg, S.-A. Influence of trace metal release from volcanic ash on growth of *Thalassiosira pseudonana* and *Emiliania huxleyi*. *Mar. Chem.* **2012**, *132*, 28–33. [[CrossRef](#)]
27. Olgun, N.; Duggen, S.; Andronico, D.; Kutterolf, S.; Croot, P.L.; Giammanco, S.; Censi, P.; Randazzo, L. Possible impacts of volcanic ash emissions of Mount Etna on the primary productivity in the oligotrophic Mediterranean Sea: Results from nutrient-release experiments in seawater. *Mar. Chem.* **2013**, *152*, 32–42. [[CrossRef](#)]
28. Browning, T.J.; Stone, K.; Bouman, H.A.; Mather, T.A.; Pyle, D.M.; Moore, M.C.; Martinez-Vicente, V. Volcanic ash supply to the surface ocean—Remote sensing of biological responses and their wider biogeochemical significance. *Front. Mar. Sci.* **2015**, *2*, 14. [[CrossRef](#)]
29. Longman, J.; Palmer, M.R.; Gernon, T.M.; Manners, H.R. The role of tephra in enhancing organic carbon preservation in marine sediments. *Earth Sci. Rev.* **2019**, *192*, 480–490. [[CrossRef](#)]
30. Watson, A.J. Volcanic iron, CO₂, ocean productivity and climate. *Nature* **1997**, *385*, 587–588. [[CrossRef](#)]
31. Hamme, R.C.; Webley, P.W.; Crawford, W.R.; Whitney, F.A.; DeGrandpre, M.D.; Emerson, S.R.; Eriksen, C.C.; Giesbrecht, K.E.; Gower, J.F.R.; Kavanaugh, M.T.; et al. Volcanic ash fuels anomalous plankton bloom in subarctic northeast Pacific. *Geophys. Res. Lett.* **2010**, *37*. [[CrossRef](#)]
32. Yevenes, M.A.; Lagos, N.A.; Fariás, L.; Vargas, C.A. Greenhouse gases, nutrients and the carbonate system in the Reloncavi Fjord (Northern Chilean Patagonia): Implications on aquaculture of the mussel, *Mytilus chilensis*, during an episodic volcanic eruption. *Sci. Total Environ.* **2019**, *669*, 49–61. [[CrossRef](#)]
33. Sun, X.; Sun, W. How will volcanic ash from the Tonga volcano eruption perturbate marine carbon cycle? *Solid Earth Sci.* **2022**, *7*, 1–4. [[CrossRef](#)]
34. Longman, J.; Palmer, M.R.; Gernon, T.M. Viability of greenhouse gas removal via artificial addition of volcanic ash to the ocean. *Anthropocene* **2020**, *32*, 100264. [[CrossRef](#)]
35. Jones, M.T.; Gislason, S.R. Rapid releases of metal salts and nutrients following the deposition of volcanic ash into aqueous environments. *Geochim. Cosmochim. Acta* **2008**, *72*, 3661–3680. [[CrossRef](#)]

36. Berezovskaya, V.A. *Hydrochemical Regime of the Avacha Bay*; Avtoref. dis. . . . kand. geogr.nauk: Rostov-na-Donu, Russia, 1988; 25p. (In Russian)
37. Berezovskaya, V.A. *Avacha Bay. Hydrochemical Regime, Anthropogenic Impact*; KGARF: Petropavlovsk-Kamchatsky, Russia, 1999; 156p. (In Russian)
38. Lepskaya, E.V.; Tepnin, O.B.; Kolomeitsev, V.V.; Ustimenko, E.A.; Sergeenko, N.V.; Vinogradova, D.S.; Sviridenko, V.D.; Pokhodina, M.A.; Shchegolkova, V.A.; Maksimenkov, V.V.; et al. Historical review of research and the main results of the complex environmental monitoring of Avacha Bay in 2013. *Res. Water Biol. Resour. Kamchatka Northwestern Part Pac. Ocean* **2014**, *34*, 5–21. Available online: <https://cyberleninka.ru/article/n/istoricheskiy-obzor-issledovaniy-i-osnovnye-rezultaty-kompleksnogo-ekologicheskogo-monitoringa-avachinskoy-guby-v-2013-g/viewer> (accessed on 1 March 2023). (In Russian).
39. Orlova, T.Y.; Aleksanin, A.I.; Lepskaya, E.V.; Efimova, K.V.; Selina, M.S.; Morozova, T.V.; Stonik, I.V.; Kachur, V.A.; Karpenko, A.A.; Vinnikov, K.A.; et al. A massive bloom of *Karenia* species (Dinophyceae) off the Kamchatka coast, Russia, in the fall of 2020. *Harmful Algae* **2022**, *120*, 102337. [[CrossRef](#)]
40. Piip, B.I. Eruption of Avacha Sopka in 1945. *Bull. Volcano* **1953**, 6–23, Art., 17. Available online: <http://repo.kscnet.ru/1558/> (accessed on 1 March 2023). (In Russian).
41. Kuksina, L. Variations of Water Runoff and Suspended Sediment Yield in the Kamchatsky Krai, Russia. *Water* **2018**, *10*, 1451. [[CrossRef](#)]
42. Vaskovsky, M.G. *Resursy Poverkhnostnykh vod SSSR Kamchatka V 20 Kamchatka*; Gidrometeoizdat: Leningrad, Russia, 1973. (In Russian)
43. Tishchenko, P.; Zhang, J.; Pavlova, G.; Tishchenko, P.; Sagalaev, S.; Shvetsova, M. Revisiting the Carbonate Chemistry of the Sea of Japan (East Sea): From Water Column to Sediment. *J. Mar. Sci. Eng.* **2022**, *10*, 438. [[CrossRef](#)]
44. Dickson, A.G. pH scales and proton-transfer reactions in saline media such as sea water. *Geochim. Cosmochim. Acta* **1984**, *48*, 2299–2308. [[CrossRef](#)]
45. Pavlova, G.Y.; Tishchenko, P.Y.; Volkova, T.I.; Dickson, A.; Wallmann, K. Intercalibration of Bruevich’s method to determine the total alkalinity in seawater. *Oceanology* **2008**, *48*, 438–443. [[CrossRef](#)]
46. Grasshoff, K.; Ehrhard, M.; Kremling, K. *Methods of Seawater Analysis*; Verlag Chemie: Weinheim, Germany, 1983; p. 419. Available online: https://scholar.google.com/scholar_lookup?title=Methods+of+Seawater+Analysis&author=Grasshoff,+K.&author=Ehrhard,+M.&author=Kremling,+K.&publication_year=1983 (accessed on 1 March 2023).
47. Martin, J.-M.; Meybeck, M. Elemental mass-balance of material carried by major world rivers. *Mar. Chem.* **1979**, *7*, 173–206. [[CrossRef](#)]
48. Litvinenko, Y.S.; Zakharikhina, L.V. Chemical transformation of Kamchatka soils after input of products of volcanic eruption. *Contemp. Probl. Ecol.* **2017**, *10*, 686–699. [[CrossRef](#)]
49. Nakano, T.; Yamada, Y.; Shin, K.-C. Effects of snow and land modification on an andesite lava aquifer in Chokai volcano, northwestern Japan. *J. Hydrol.* **2022**, *612*, 128191. [[CrossRef](#)]
50. Cheshko, A.L. The formation of the main types of thermal waters of the Kuril-Kamchatka region based on the isotopic studies (D, ¹⁸O, ³He/⁴He). *Geochemistry.* **1994**, *7*, 988–1001. (In Russian)
51. Mikhailik, T.A.; Tishchenko, P.Y.; Koltunov, A.M.; Tishchenko, P.P.; Shvetsova, M.G. The effect of Razdol’naya River on the environmental state of Amur Bay (the Sea of Japan). *Water Res.* **2011**, *38*, 512–521. [[CrossRef](#)]
52. Sugimoto, R.; Tsuboi, T.; Fujita, M.S. Comprehensive and quantitative assessment of nitrate dynamics in two contrasting forested basins along the Sea of Japan using dual isotopes of nitrate. *Sci. Total Environ.* **2019**, *687*, 667–678. [[CrossRef](#)]
53. Zhang, P.; Ruan, H.; Dai, P.; Zhao, L.; Zhang, J. Spatiotemporal river flux and composition of nutrients affecting adjacent coastal water quality in Hainan Island, China. *J. Hydrol.* **2020**, *591*, 125293. [[CrossRef](#)]
54. Semkin, P.Y.; Tishchenko, P.Y.; Pavlova, G.Y.; Tishchenko, P.P.; Sagalaev, S.G.; Shkirknikova, E.M.; Shvetsova, M.G. The Carbonate System of the Estuaries of the Syran and Ul’ban Rivers (Ul’banskii Bay, the Sea of Okhotsk) during Spring Flood. *Water Res.* **2022**, *49*, 869–8791. [[CrossRef](#)]
55. Ayris, P.M.; Delmelle, P. The immediate environmental effects of tephra emission. *Bull. Volcanol.* **2012**, *74*, 1905–1936. [[CrossRef](#)]
56. Galeczka, I.; Sigurdsson, G.; Eiriksdottir, E.S.; Oelkers, E.H.; Gislason, S.R. The chemical composition of rivers and snow affected by the 2014/2015 Bárðarbunga eruption, Iceland. *J. Volcanol. Geotherm. Res.* **2016**, *316*, 101–119. [[CrossRef](#)]
57. Mouri, G.; Che Ros, F.; Chalov, S. Characteristics of suspended sediment and river discharge during the beginning of snowmelt in volcanically active mountainous environments. *Geomorphology* **2014**, *213*, 266–276. [[CrossRef](#)]
58. Taran, Y.A.; Ryabinin, G.V.; Pokrovsky, B.G.; Nazhalova, I.N.; Malik, N.A. Mineral waters of the Avacha depression. *Vestnik KRAUNTS. Earth Sci.* **2021**, *50*, 22–39. (In Russian) [[CrossRef](#)]
59. Zakharkov, S.P.; Lepskaya, Y.V.; Tepnin, O.B.; Shtraykhert, Y.A.; Gordeychuk, T.N. Pervichnaya produktsiya Avachinskoy bukhty letom 2017. *Vestn. Dal’nevostochnogo Otd. Ross. Akad. Nauk.* **2020**, *1*, 83–89. Available online: <http://vestnikdvo.ru/index.php/vestnikdvo/article/view/523> (accessed on 1 March 2023). (In Russian).
60. Zvalinsky, V.I.; Tishchenko, P.P.; Mikhailik, T.A.; Tishchenko, P.Y. Eutrophication of the Peter the Great Bay. In *Oceanographic Studies of the Far Eastern Seas and the North-Western of the Pacific*; Akulichhev, V.A., Ed.; Dalnauka: Vladivostok, Russia, 2013; pp. 260–293. (In Russian)
61. Sterner, R.W.; Elser, J.J. *Ecological stoichiometry*. In *Ecological Stoichiometry*; Princeton University Press: Princeton, NJ, USA, 2017.
62. Li, X.; Yan, T.; Yu, R.; Zhou, M. A review of *karenia mikimotoi*: Bloom events, physiology, toxicity and toxic mechanism. *Harmful Algae* **2019**, *90*, 101702. [[CrossRef](#)]

63. Talley, L.D. *Hydrographic Atlas of the World Ocean Circulation Experiment (WOCE). V. 2: Pacific Ocean*; Sparrow, M., Chapman, P., Gould, J., Eds.; International WOCE Project Office: Southampton, UK, 2007.
64. Ruttenberg, K.C.; Sulak, D.J. Sorption and desorption of dissolved organic phosphorus onto iron (oxyhydr) oxides in seawater. *Geochim. Cosmoch. Acta* **2011**, *75*, 4095–4112. [[CrossRef](#)]
65. Froelich, P.N. Kinetic control of dissolved phosphate in natural rivers and estuaries: A primer on the phosphate buffer mechanism. *Limnol. Oceanogr.* **1988**, *30*, 649–668. [[CrossRef](#)]
66. Mort, H.P.; Slomp, C.P.; Gustafsson, B.G.; Andersen, T.J. Phosphorus recycling and burial in Baltic Sea sediments with contrasting redox conditions. *Geochim. Cosmochim. Acta* **2010**, *74*, 1350–1362. [[CrossRef](#)]
67. Malik, N.A. Impaktny contribution of volcanic eruptions to formation of the chemical composition of seasonal snow cover (Kamchatka). *Ice and snow*. **2010**, *4*, 45–52. (In Russian)
68. Kim, S.-H.; Lee, J.-S.; Kim, K.-T.; Kim, H.-C.; Lee, W.-C.; Choi, D.; Choi, S.-H.; Choi, J.-H.; Lee, H.-J.; Shin, J.-H. Aquaculture Farming Effect on Benthic Respiration and Nutrient Flux in Semi-Enclosed Coastal Waters of Korea. *J. Mar. Sci. Eng.* **2021**, *9*, 554. [[CrossRef](#)]

Disclaimer/Publisher’s Note: The statements, opinions and data contained in all publications are solely those of the individual author(s) and contributor(s) and not of MDPI and/or the editor(s). MDPI and/or the editor(s) disclaim responsibility for any injury to people or property resulting from any ideas, methods, instructions or products referred to in the content.